Research Inventy: International Journal of Engineering and Science
Vol.16, Issue 8 (August 2026), PP 01-12
Issn (e): 2278-4721, Issn (p):2319-6483, www.researchinventy.com

Simulation and optimization of Y-tube design using the Taguchi-Gray method.

Ut Hien Nguyen Thi*, Trong Hieu Nguyen, Thanh Dat Vo, Quoc Ngoc Tran, Thanh Hung Phan.

Faculty of Mechanical Engineering and Technology, Ho Chi Minh City University of Industry and Trade, 140 Le Trong Tan Street, Tay Thanh Ward, Ho Chi Minh City, Vietnam, 700000
Corresponding Author: Ut Hien Nguyen Thi (hienntu@huit.edu.vn)

Abstract: *In automatic coffee vending machines, the Y-shaped mixing tube plays a crucial role in transporting hot water and coffee grounds to the extraction chamber, directly impacting brewing efficiency and system durability. This study utilizes combined CFD and Static Structural numerical simulation to evaluate the flow characteristics, pressure distribution, stress, and strain of the Y-shaped tube under real-world operating conditions. The simulation results are used to determine the optimal configuration to minimize pressure loss, reduce coffee grounds clogging, and minimize stress and strain on the component. This research contributes to improving beverage quality, increasing system durability, and providing a scientific basis for the design and optimization of automatic coffee vending machines.*

Keywords: *Y-tube; CFD; Static Structural; stress; strain; automatic coffee vending machine.*

Date of Submission: 24-07-2026 Date of Acceptance: 06-08-2026

I. INTRODUCE

In recent decades, vending machine systems have become an essential platform in the service industry, providing continuous service and a high degree of automation, as demonstrated in studies by Ana Monga and Balwinder Singh (2012) and Melissa A. Matthews et al. Tanya M. Horacek (2015). In particular, automatic coffee machines are becoming increasingly popular. However, due to their continuous and demanding operating environment, these systems are susceptible to mechanical and physical problems such as wear on moving parts, corrosion of solenoid valves, pressure fluctuations, and degradation of extraction efficiency over time. To address these issues, numerous improvements in brewing mechanism design, structural optimization, and process control have been studied to enhance system reliability and stability, as confirmed by Barella et al. (2013) and Taşpınar & Akbari (2025). Although automation technologies have rapidly developed through the works of Illy and Viani (2005) and Navarini et al. (2009), practical brewing mechanisms still face many challenges in operation. Common problems include clogging of the coffee grounds due to uneven particle size distribution, the formation of flow channels reducing extraction efficiency, and the risk of leaks at joints and pipes when the system has to operate under high pressure and prolonged hot water temperatures. Historically, design processes for mixing mechanisms have often prioritized experimental methods and the fabrication of actual prototypes due to their intuitiveness and the ability to quickly assess product effectiveness. However, according to Versteeg and Malalasekera (2007), these methods are primarily based on experimental results, making it difficult to fully explain the internal physical mechanisms of the system and requiring significant time and cost for design optimization. Therefore, modern research has shifted to the application of numerical modeling and multi-physics simulation. According to Ferziger and Perić (2002), combining computational fluid dynamics (CFD), heat transfer, and structural mechanics analysis allows for the simultaneous description of flow phenomena, heat transfer, and stress distribution within the device, thereby supporting design optimization with higher accuracy. To solve the differential equations describing the interaction between velocity, pressure, and temperature fields during the brewing process, numerical simulation software such as ANSYS Fluent has become an important tool in the analysis and design of thermal fluid systems. In particular, Xu et al. (2025) applied ANSYS to combine heat transfer analysis and structural analysis for a coffee brewing mechanism, thereby evaluating the stress and strain distribution under the simultaneous influence of mechanical load and temperature. The research results showed that integrating multi-physics models improves the accuracy in predicting stress concentration regions, while also supporting structural optimization and improving equipment durability. Furthermore, Versteeg and Malalasekera (2007) confirmed that computational fluid dynamics methods allow for the simultaneous solution of mass, momentum, and energy conservation equations, thereby accurately predicting the distribution of velocity, pressure, and temperature fields in the system. Thanks to its ability to simulate heat transfer and flow phenomena in detail, CFD contributes to optimizing design, reducing pressure losses, limiting coffee grounds buildup in pipelines, and improving the reliability and lifespan of the brewing unit. Although designs based on real-world testing exhibit high compatibility with operating conditions, their "black box" nature fails to fully explain the internal physical mechanisms of the Y-tube assembly during the dispensing process. To overcome this limitation, this study employs a multi-physics simulation approach, enabling detailed description of complex heat transfer interactions, flow dynamics, and mechanical strength. Using the finite element method in Ansys, control equations for mass, momentum, and energy conservation are solved simultaneously. This method ensures accurate prediction of flow dynamics, providing a solid foundation for optimizing Y-tube assembly design and effectively addressing clogging and cracking issues in automated dispensing machines.

II. RESEARCH METHODS

2.1. Establishing the physical model and boundary conditions

The 3D model of the Y-shaped pipe assembly was designed using Autodesk Inventor software, comprising a vertical branch carrying hot water and a secondary branch inclined at 45 degrees carrying coffee grounds. In the ANSYS Static Structural simulation environment, boundary conditions were set to closely resemble real-world operating conditions:

Fixing condition: The two outlet pipe openings and the flange section are fixed together using a Fixed Support tool.

Inlet load: The hot water branch is subjected to a pressure of 9 bar and a temperature of 366K.

2.1.1. Geometric Model and Computational Domain

The geometric shape is based on the actual specifications of the Express coffee machine.

Figure 1: Parameters of the Y-shaped tube

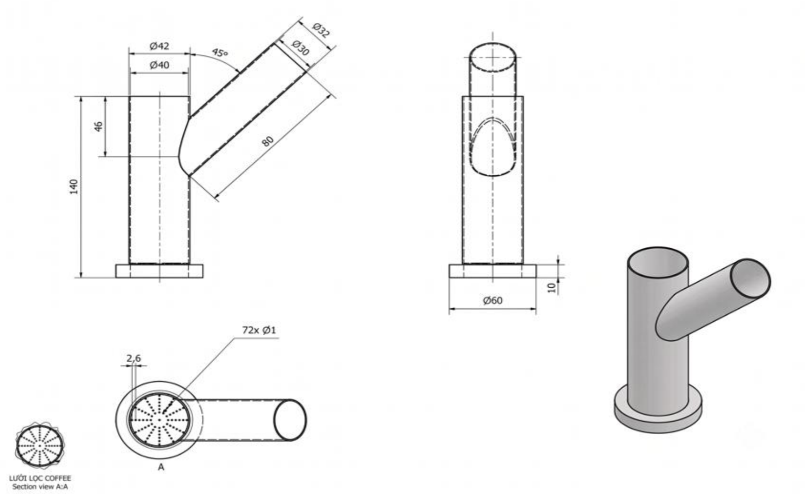

The Y-shaped tube has a total length of 140mm, a straight tube diameter of Ø42mm, a branch tube diameter Øof 32mm, and a branch tube length of 80mm, with a filter mesh pore size of Ø1mm.

2.1.2. Grid control and time step

Mesh type: An unstructured tetrahedral element mesh with high element density is used. The mesh is set fine enough to closely follow the geometric profile of the Y-tube, thereby helping to control analysis errors and ensuring convergence conditions for strongly coupled nonlinear equations.

Figure 2: Grid model of the Y-shaped tube.

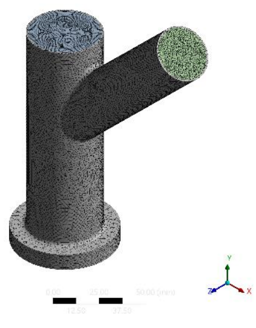

Mesh parameters: Element size is 2 mm, minimum is 0.0272 mm. Element growth rate is limited to 1.2 with a curvature coefficient of 0.3, resulting in 3577313 nodes and 1710435 elements, ensuring high convergence and reliability for static simulation.

The numerical simulation was conducted under steady-state conditions to evaluate the final stabilized flow field and pressure distribution within the Y-tube. The Coupled pressure-velocity coupling scheme was employed to accelerate convergence and ensure stability for the highly non-linear mass and momentum equations. To minimize numerical diffusion and maintain high accuracy, the Second Order Upwind spatial discretization scheme was applied to both momentum and energy equations. The calculation was set for up to 1000 iterations to guarantee strict convergence criteria.

Figure 3: Grid-like image of the Y-shaped tube.

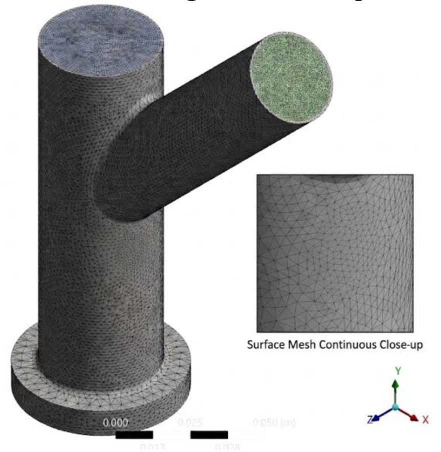

Figure 4 illustrates the geometric model setup and the applied boundary conditions for the fluid domain. As depicted, the two upper openings serve as the inlets for the system, indicated by the inward-pointing blue arrows. Specifically, the vertical branch is designated for the hot water flow, while the 45-degree inclined branch facilitates the entry of the coffee grounds. Conversely, the flanged opening at the bottom acts as the pressure outlet for the extracted mixture, represented by the outward-pointing red arrows. This configuration accurately reflects the real-world mass flow direction within the automated brewing mechanism, establishing a highly reliable foundation for the subsequent numerical analysis.

Figure 4: Fluent module view

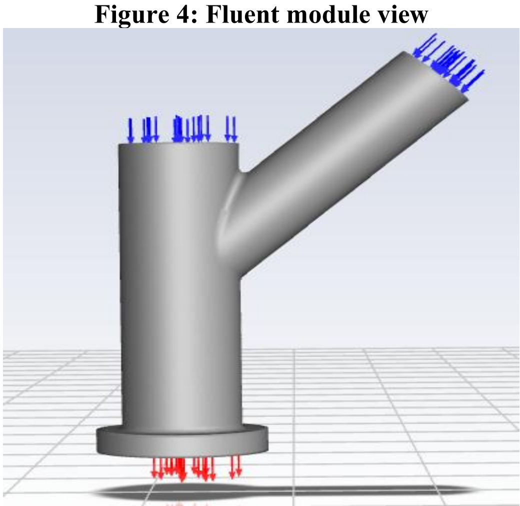

2.1.3. Design of the Y-shaped pipe model

The Y-shaped pipe model in this study was designed using Autodesk Inventor software.
Based on the standard specifications of a 304 stainless steel coffee filter press assembly, the overall dimensions are selected with four main design variables:

Table 1: Design variables and levels

Improved responses	Symbol	Unit	Level 1	Level 2	Level 3
Main hot water pipe diameter	DO	mm	42	47	52
Diameter of the auxiliary pipe for conveying coffee powder.	DP	mm	32	37	42
Filter mesh hole diameter	SL	mm	1	1.4	1.8
Length of the main hot water pipe	LO	mm	140	145	150

2.2. Method for determining MEREC weights

The weight of each objective, which is determined by the MEREC method (Borchers & Pieler, 2010; Fan et al., 2024; Keshavarz-Ghorabaee, 2021; Keshavarz-Ghorabaee et al., 2021; Shanmugasundar et al., 2022) as following:

Determine performance for each case

$$S_i = \ln\left[1 + \left(\frac{1}{n}\sum_{j}^{n}\left|\ln(h_{ij})\right|\right)\right] \tag{1}$$

Determine effective performance after removing single criteria

$$S_{ij}^{'} = \ln\left[1 + \left(\frac{1}{n}\sum_{k,k\neq j}^{n}\left|\ln(h_{ij})\right|\right)\right] \tag{2}$$

Determine the deviation of the criteria

$$E_j = \left|S_{ij}^{'} - S_i\right| \tag{3}$$

Determine the weight for each objective

$$w_j = \frac{E_j}{\sum_k^m E_k} \tag{4}$$

Normalize the decision matrix for maximization goals:

$$h_{ij} = \frac{u_{ij}}{\max u_{ij}} \tag{5}$$

2.2.1. Grey's Relationship Analysis Method

To confirm the optimal values of strain and stress, the GRA method is applied in the following sequence:

Normalize data using the Larger is Better criterion for the signal-to-noise ratio:

$$\boldsymbol{x_i^*(k) = \frac{x_i^{(0)}(k) - min x_i^{(0)}(k)}{max\, x_i^{(0)}(k) - min x_i^{(0)}(k)}} \tag{6}$$

Calculate the Grey relation coefficient:

$$\boldsymbol{\gamma_i(k) = \frac{\Delta_{min} + \zeta\, \Delta_{max}}{\Delta_{0i}(k) + \zeta\, \Delta_{max}}} \tag{7}$$

2.2.2. Taguchi Method

To confirm the influence of design variables on the strain and stress of the proposed model through FEA analysis, the Taguchi method was used. The objective of optimizing strain and stress according to the Larger is Better system was calculated using the signal-to-noise ratio (S/N) equation as follows:

$$S/N = -10\,log\left(\frac{1}{n}\sum_{i=1}^{n}\frac{1}{y_i^2}\right) \tag{8}$$

$$CI_{CE} = \pm\sqrt{F_{\alpha}(1, fe)Ve\left(\frac{1}{n_{eff}} + \frac{1}{R_e}\right)} \tag{9}$$

$F_{\alpha}(1, fe)$ obtained by Table B-2 (Roy, 2010) .

2.3. Boundary Conditions

The boundary conditions are set as follows.

- Hot water inlet

Velocity: 0 m/s

Temperature: 366.5 ° K

Phase pressure: 9 bar

- Coffee powder inlet

Velocity: 0.05 m/s
The coffee powder layer is modeled using Porous Zone.
- Exit
+ Pressure Outlet
+ Gauge Pressure 0 Pa

Table 2: Key parameters used in the simulation model

Symbol	Parameter	Value	Unit
304 stainless steel			
ρ	Density	8030 K g/ m^3	ASM Handbook, Stainless Steel 304
C_p	Specific Heat	500 J / (kg.K)	ASM Handbook
k	Elevated Conduct	16.2 (W/ mK)	ASM Handbook
Water hot			
ρ	Density	963.3 K g/ m^3	IAPWS-95 / IAPWS Liquid Water
C_p	Specific Heat	4208 J / (kg.K)	Experiment
k	Elevated Conduct°	0.676 (W/ mK)	IAPWS Thermal Conductivity
μ	Dynamic Viscosity	0.000315 kg/(m·s) (Pa·s)	IAPWS Viscosity
Coffee_bed			
ρ	Density	500 K g/ m^3	Physical and thermal properties of coffee
C_p	Specific Heat	1006.43 J / (kg.K)	-
k	Elevated Conduct	0.016 (W/ mK)	-

III. RESULTS AND DISCUSSION

3.1. Flow characteristics and pressure distribution analysis

3.1.1. Total pressure distribution

Figure 5 presents the total pressure distribution contour within the Y-tube assembly during the fluid mixing phase. The CFD simulation reveals a distinct pressure gradient, with the maximum total pressure reaching $3.28x10^2$ Pa at the inlet of the inclined branch, which is responsible for supplying the coffee grounds. As the flow travels towards the intersection, the pressure gradually decreases, facilitating a smooth transport mechanism. Notably, a localized negative pressure zone reaching up to $-1.97x10^2$ Pa is observed at the upper section of the vertical main pipe. This specific pressure differential induces a suction effect at the junction, effectively drawing the fluid and powder mixture downward while preventing the backflow or accumulation of coffee grounds at the top of the vertical tube. Consequently, this pressure distribution confirms the aerodynamic efficiency of the 45° inclined design in mitigating clogging risks within the automated dispensing system.

Figure 5: Total pressure distribution contour in the Y-shaped mixing tube

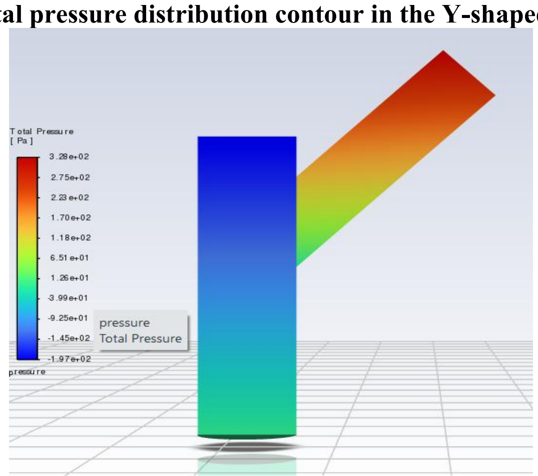

3.1.2. Thermal interaction and temperature distribution

Figure 6 illustrates the velocity vectors colored by total temperature within the Y-tube assembly, providing detailed insight into the fluid dynamics and thermal interaction during the brewing process. As observed, the incoming coffee grounds from the inclined branch maintain an ambient temperature of approximately 3.00 x10^2 ^{o} K blue vectors, while the vertical branch introduces hot water at 3.66x10^2 ^{o}K red-orange vectors. Upon converging at the intersection, the high-temperature fluid rapidly transfers heat to the coffee particles, resulting in a swift thermal elevation. The mixed stream maintains an elevated and stable temperature toward the outlet, ensuring optimal thermal conditions for extraction. Furthermore, the directional alignment of the vectors confirms a smooth, continuous flow path without stagnant zones or flow reversal, validating the aerodynamic efficiency of the proposed 45^o inclined configuration.

Figure 6: Thermal distribution and flow vectors during the mixing process inside the Y-tube

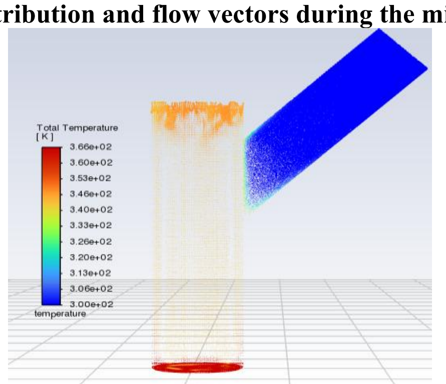

3.1.3. Velocity field and flow dynamics analysis

Figure 7 illustrates the velocity magnitude distribution and flow vectors within the Y-tube assembly. The simulation results indicate that the flow velocity reaches a maximum magnitude of approximately 6.43x10^{-2} m/s. The vector distribution demonstrates a smooth and continuous transition of the fluid from the upper inlets toward the lower outlet. This controlled velocity profile confirms the absence of severe stagnation zones or excessive recirculation, ensuring efficient transport of the coffee mixture and verifying the hydrodynamic stability of the designed system.

Figure 7: Velocity magnitude distribution and vector field in the Y-tube assembly

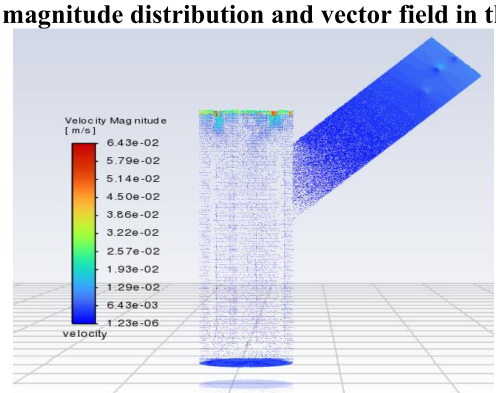

3.1.4. Flow characteristics and pressure distribution analysis

Figure 8 presents the velocity vectors colored by total pressure within the Y-tube assembly, delineating the pressure drop and flow dynamics during operation. As indicated by the color gradient, the total pressure reaches a maximum of approximately 4.93x10^3 Pa at the inlet of the inclined branch, progressively decreasing as the flow converges toward the main vertical channel and exits the system. This clear pressure differential validates the driving force required for the smooth transport of the mixture, confirming that the designed geometry effectively prevents excessive pressure accumulation and flow resistance.

Figure 8: Total pressure field represented via velocity vectors in the automated Y-tube mechanism

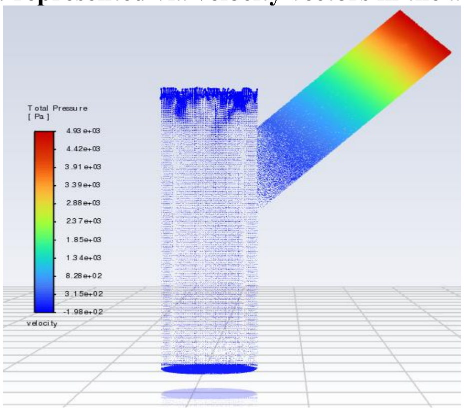

3.2. Structural optimization and multi-criteria decision making

The finite element analysis results of 27 models recorded 27 strain values and 27 stress values, as shown in Table 3. In this table, the stress and strain values of the 27 cases are completely different. This demonstrates that the design variables considered are crucial, as they significantly altered the strain and stress values.

Table 3: The results of finite element analysis for 27 cases.

SL	DO	DP	LO	DEF (mm)	STRESS (MPa)
1	42	32	140	2.55E-05	0.068873
1	42	37	145	3.08E-05	0.08615
1	42	42	150	5.19E-05	0.090773
1	47	32	145	2.93E-05	0.051823
1	47	37	150	3.158E-05	0.062804
1	47	42	140	3.31E-05	0.073383
1	52	32	150	3.69E-05	0.043227
1	52	37	140	3.65E-05	0.045169
1	52	42	145	3.79E-05	0.053048
1.4	42	32	140	2.57E-05	0.068781
1.4	42	37	145	3.09E-05	0.086001
1.4	42	42	150	5.19E-05	0.090624
1.4	47	32	145	2.95E-05	0.051975
1.4	47	37	150	3.17E-05	0.062753
1.4	47	42	140	3.32E-05	0.07422
1.4	52	32	150	3.71E-05	0.041402
1.4	52	37	140	3.68E-05	0.045046
1.4	52	42	145	3.83E-05	0.052964
1.8	42	32	140	2.58E-05	0.06879
1.8	42	37	145	3.10E-05	0.085797
1.8	42	42	150	5.17E-05	0.090396
1.8	47	32	145	2.97E-05	0.051876
1.8	47	37	150	5.97E-06	0.021768
1.8	47	42	140	3.34E-05	0.074073
1.8	52	32	150	3.75E-05	0.042148
1.8	52	37	140	3.72E-05	0.044965
1.8	52	42	145	3.87E-05	0.052809

3.3. Weighting results

The weights were determined by the MEREC method, as recorded in Table 4. In this Table, the normalized values of Di and St are recorded in the second and third columns obtained by substituting 27 strain values and 27 stress values into Equation (2). The fourth column is obtained by Equation (1). The fifth and sixth columns are obtained by Equation (2). The seventh and eighth columns are obtained by Equation (3). Weights of strain and stress
The yields obtained are 0.3935 and 0.5300 respectively by Equation (4).

Table 4: Weighting results

hij			Sij'		Ej	
Di	St	Si	Di	St	Di	St
0.4913	0.3161	0.6582	0.3041	0.4548	0.3541	0.1508
0.5935	0.2527	0.6671	0.2318	0.5234	0.4354	0.2916
1.0000	0.2398	0.5388	0.0000	0.5388	0.5388	0.5388
0.5649	0.4201	0.5419	0.2512	0.3603	0.2907	0.1090
0.6082	0.3466	0.5757	0.2220	0.4251	0.3537	0.2031
0.6373	0.2966	0.6059	0.2032	0.4748	0.4027	0.2716
0.7098	0.5036	0.4150	0.1582	0.2949	0.2568	0.1367
0.7029	0.4819	0.4326	0.1624	0.3111	0.2702	0.1488
0.7307	0.4104	0.4714	0.1457	0.3684	0.3257	0.2227
0.4941	0.3165	0.6564	0.3020	0.4544	0.3544	0.1524
0.5950	0.2531	0.6661	0.2308	0.5229	0.4353	0.2921
0.9988	0.2402	0.5387	0.0006	0.5383	0.5381	0.5377
0.5675	0.4188	0.5414	0.2494	0.3613	0.2920	0.1119
0.6107	0.3469	0.5743	0.2204	0.4249	0.3539	0.2045
0.6395	0.2933	0.6081	0.2018	0.4783	0.4063	0.2765
0.7147	0.5258	0.3983	0.1552	0.2787	0.2431	0.1235
0.7083	0.4832	0.4292	0.1591	0.3101	0.2701	0.1510
0.7382	0.4110	0.4677	0.1413	0.3678	0.3264	0.2265
0.4974	0.3164	0.6547	0.2995	0.4544	0.3552	0.1549
0.5972	0.2537	0.6645	0.2293	0.5222	0.4352	0.2929
0.9962	0.2408	0.5387	0.0019	0.5376	0.5368	0.5357
0.5712	0.4196	0.5390	0.2469	0.3606	0.2921	0.1137
0.1150	1.0000	0.7331	0.7331	0.0000	0.0000	0.7331
0.6438	0.2939	0.6057	0.1990	0.4777	0.4067	0.2786
0.7218	0.5165	0.4010	0.1510	0.2855	0.2500	0.1345
0.7155	0.4841	0.4253	0.1547	0.3095	0.2706	0.1547
0.7454	0.4122	0.4637	0.1371	0.3668	0.3267	0.2297

3.4. Grey method results

To determine the ideal design configuration, an optimal model must simultaneously satisfy rigorous criteria: low stress, minimal deformation, and a lightweight structure. Based on these engineering criteria, the

Grey Relational Grade method was applied to select the most optimal model. The optimization analysis results obtained using the GRG method are comprehensively recorded in Table 5. Specifically, the normalized grey relational values for the evaluation criteria regarding stress (Di) and deformation (Si) are presented in the first and second columns under the corresponding weight Wj, respectively. The third column displays the GRG simulation value for each case, while the final column indicates their priority rank. According to the evaluation principles, the highest GRG simulation value is ranked first and identified as the optimal case of the entire study. Based on the results, case 3 demonstrated absolute superiority and was selected as the optimal configuration. The optimal GRG simulation value achieved was 1.0000, demonstrating that this approach provides the best balance between mechanical strength, load-bearing capacity, and structural weight optimization.

Figure 9: Equivalent stress model 3

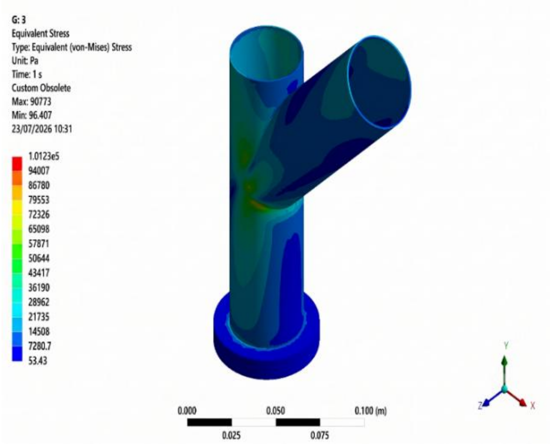

Figure 10: Overall profile of model number 3

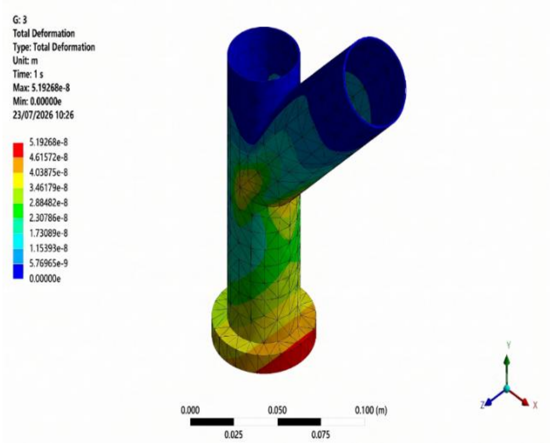

Table 5: GRG value and rank

wj		GRG simulation	Rank
Di	St		
0.5790	0.4210	0.5269	17
0.5570	0.4116	0.6731	4
0.5300	0.3935	1.0000	1
0.4965	0.3600	0.4896	22
0.4784	0.3533	0.5396	12
0.4565	0.3407	0.5981	8
0.4314	0.3238	0.5267	18
0.4155	0.3153	0.5276	15
0.3987	0.3060	0.5612	10
0.3785	0.2922	0.5271	16
0.3565	0.2827	0.6721	5
0.3294	0.2646	0.9972	2
0.2960	0.2312	0.4909	21
0.2779	0.2242	0.5403	11
0.2559	0.2115	0.6037	7
0.2306	0.1944	0.5254	19
0.2155	0.1867	0.5298	13

0.1988	0.1773	0.5645	9
0.1785	0.1632	0.5281	14
0.1564	0.1536	0.6712	6
0.1294	0.1354	0.9913	3
0.0960	0.1022	0.4917	20
0.0779	0.0951	0.3333	25
0.0779	0.0495	0.3960	23
0.0526	0.0322	0.3342	24
0.0371	0.0239	0.3333	25
0.0203	0.0143	0.3333	25

3.5. Taguchi method results

Table 6: Signal to Noise Ratios of Vi

Level	SL	D0	DP	LO
1	-4.113	-2.551	-5.776	-5.577
2	-4.110	-5.672	-5.268	-4.883
3	-6.633	-6.633	-3.812	-4.395
Delta	2,523	4,082	1,963	1,182
Rank	2	1	3	4

Figure 11: Primary effect diagram for SN ratio

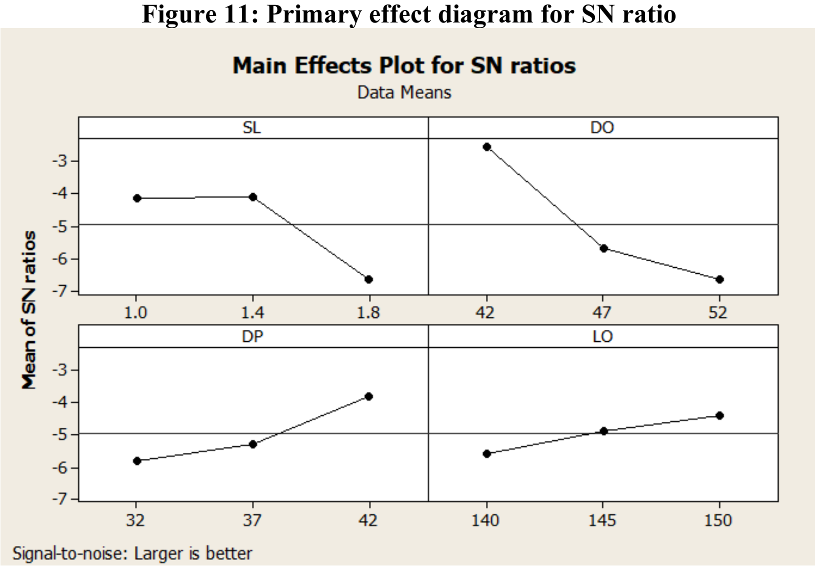

Figure 12: The graph interaction analysis of Vi signal to noise

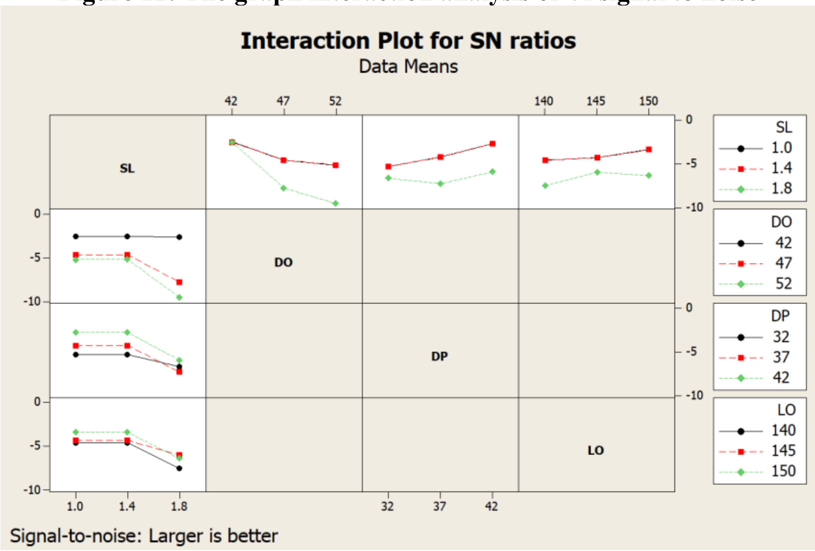

IV. CONCLUSION

This study has successfully developed and applied a finite element model using the ANSYS platform, integrated with the Taguchi-GRA-MEREC multi-objective optimization algorithm, to comprehensively resolve the design problem of the Y-shaped pipe assembly for automatic coffee vending machines. The simulation results affirm that geometric design variables have a direct and profound impact on the stress field and deformation distribution within the component, including the main pipe diameter (DO) is identified as the most dominant factor governing the load-bearing capacity of the entire structure. The consistent convergence between the signal-to-noise (S/N) ratio analysis and the multi-criteria decision-making method has proven the absolute superiority of design configuration No. 3 (with SL = 1 mm, DO = 42 mm, DP = 42 mm, and LO = 150 mm), achieving the maximum Gray Relational Grade (GRG) value of 1.0000. This comprehensive theoretical framework not only verifies the stability of the proposed approach but also provides a powerful analytical tool to optimize the mechanical design space, contributes to enhanced structural rigidity, minimized material usage, and maximized operational lifespan for industrial beverage dispensing mechatronic systems.

Conflict of interest

The authors declare they have no conflict of interest or financial conflicts to disclose.
This article contains no studies with human or animal subjects performed by authors.

ACKNOWLEDGEMENT

The authors gratefully acknowledge the research support from Ho Chi Minh City University of Industry and Trade.

REFERENCES

[1] Abhinandan Choubey, N. V. S. (2024). A Review of Optimization of Alloy Wheel Rim. International Journal of Scientific Modern Research and Technology, 16(2), 1-4.
[2] Ashok, B., Naidu, M. K., & Rao, S. S. (2021). Design and Weight Optimization of Aluminium Alloy Wheel Rim for Light Weight Four Wheeled Vehicle. International Journal of Engineering Research & Technology, 10(4), 484-490.
[3] Barragán-Trinidad, M., Guadarrama-Pérez, O., Guillén-Garcés, R. A., Bustos-Terrones, V., Trevino-Quintanilla, L. G., & Moeller-Chávez, G. (2023). The Grey–Taguchi Method, a Statistical Tool to Optimize the Photo-Fenton Process: A Review. Water, 15(15), 1-27.
[4] Borchers, A., & Pieler, T. (2010). Programming pluripotent precursor cells derived from Xenopus embryos to generate specific tissues and organs. Genes (Basel), 1(3), 413-426.
[5] Ciardiello, F., & Genovese, A. (2023). A comparison between TOPSIS and SAW methods. Annals of Operations Research, 325(2), 967-994.
[6] Danzi, N., Solazzi, L., & Cima, M. (2024). Development of a FEM procedure for evaluating the pressure profile in the industrial wheel and fatigue strength analyses. Journal of Applied Engineering Science, 22(2), 171-183.
[7] Fan, J., Lei, T., & Wu, M. (2024). MEREC-MABAC method based on cumulative prospect theory for picture fuzzy sets: Applications to wearable health technology devices. Expert Systems with Applications, 255, 414-422.
[8] Gadwala, W. K., & Babu G, R. (2022). Modeling and analysis of car wheel rim for weight optimization to use additive manufacturing process. Materials Today: Proceedings, 62, 336-345.
[9] Jakupi, K., Dukovski, V., & Abdullahu, F. (2024). Optimizing surface roughness of workpieces made of stainless steel 316L with DMLS technology: a Taguchi method approach. Engineering Research Express, 6(2), 1-7.
[10] Kepekci, H., Agca, M., & Komatina, M. (2025). Thermal and mechanical analysis of wheel rim in Formula 1 vehicles. Thermal Science, 29(1 Part A), 325-335.
[11] Keshavarz-Ghorabaee, M., Amiri, M., Zavadskas, E. K., Turskis, Z., & Antucheviciene, J. (2021). Determination of Objective Weights Using a New Method Based on the Removal Effects of Criteria (MEREC). Symmetry, 13(4), 525.

[12] Kruzel, R., Dembiczak, T., & Wachowicz, J. (2023). Optimization of Spark Plasma Sintering Technology by Taguchi Method in the Production of a Wide Range of Materials: Review. Materials (Basel), 16(16), 1-18.
[13] Loganathan, K., & Vijaya Siva Subramani, S. K. (2023). Design and optimization of aluminium alloy wheel rim in automobile industry. Materials Today: Proceedings.
[14] Majumder, H., Sheshrao Gajghate, S., Rameshchandra Sahu, A., Kumar Behera, A., Limbadri, C., & Ukey, K. (2023). Finite element analysis of wheel rim by additive manufacturing materials. Materials Today: Proceedings, 28, 341-349.
[15] Montassir, S., Moustabchir, H., El Khalfi, A., Vlase, S., & Scutaru, M. L. (2024). Numerical Study of Crack Prediction and Growth in Automotive Wheel Rims. Materials (Basel), 17(5), 1-14.
[16] Padmanabhan, S., Boopathi, B., Kumar, K. M., J. R, D., T, V. K., & S, B. (2023). Investigation of alloy materials on a sports bike wheel rim designs using finite element analysis. Multidisciplinary Science Journal, 6(2), 1-9.
[17] Parihar, Y. P. S., & Chakraborty, A. (2022). Dynamic Design and Analysis of Car Wheel Rim Using FEA Method. International Journal for Research in Applied Science and Engineering Technology, 10(5), 723-734.
[18] Rajesh Khatiwada, Sandip Giri, Raju Khadka, & Mahat, C. (2025). Design, analysis and optimization of the wheel rim. International Journal of Research in Aeronautical and Mechanical Engineering, 13(4), 1-13.
[19] Roy, R. K. (2010). A primer on the Taguchi method. Society of Manufacturing Engineers, Second edition.
[20] Salman Alfarisi, Riyan Ariyansah, & Mugisidi, D. (2024). Finite element analysis of aluminum based r22 car wheel design modification. Asiimetrik, 6, 1-10.
[21] Santos, V. R. I., Scinocca, F., Almeida, L. G. N. d., & Santos, F. L. (2025). VIRTUAL DEVELOPMENT OF AUTOMOTIVE WHEELS: Modal, Vertical Impact and Fatigue Analysis and Simulation, using the finite element method. Theoretical and Applied Engineering, 9(1), 1-20.
[22] Shanmugasundar, G., Sapkota, G., Čep, R., & Kalita, K. (2022). Application of MEREC in Multi-Criteria Selection of Optimal Spray-Painting Robot. Processes, 10(6), 1172.
[23] Sharma, A., Yadav, R., & Sharma, K. (2021). Optimization and investigation of automotive wheel rim for efficient performance of vehicle. Materials Today: Proceedings, 45, 3601-3604.
[24] Shinde, T., Jomde, A., Shamkuwar, S., Sollapur, S., Naikwadi, V., & Patil, C. (2022). Fatigue analysis of alloy wheel using cornering fatigue test and its weight optimization. Materials Today: Proceedings, 62, 1470-1474.
[25] Song, J., & et al. (2024). Finite Element Simulation and Microstructural Analysis of Roll Forming for DP590 High-Strength Dual-Phase Steel Wheel Rims. Materials (Basel), 17(15), 1-18.
[26] Taherdoost, H. (2023). Analysis of Simple Additive Weighting Method (SAW) as a MultiAttribute Decision-Making Technique: A Step-by-Step Guide. Journal of Management Science & Engineering Research, 6(1), 21-24.
[27] Wang, Z., Wang, C., Yang, G., & Wu, F. (2022). Innovative Design of Automobile Wheel Rim Based on Honeycomb Features. Journal of Engineering Management and Systems Engineering, 1(2), 67-75.
[28] Zhang, S., Lu, D., Li, R., Xu, L., Jiang, H., Cao, Y., & Xu, W. (2023). Fatigue life optimization and lightweight design of wheel based on entropy weight grey relation analysis and modified NSGA-II. Advances in Mechanical Engineering, 15(8), 1-20.
[29] Hisam, M. W., Dar, A. A., Elrasheed, M. O., Khan, M. S., Gera, R., & Azad, I. (2024). The Versatility of the Taguchi Method: Optimizing Experiments Across Diverse Disciplines. Journal of Statistical Theory and Applications, 23(4), 365-389.
[30] Keshavarz-Ghorabaee, M. (2021).Assessment of distribution center locations using a multi-expert subjective-objective decision-making approach. Sci Rep, 11(1), 19461.